Electromagnetic Stirrer Operating in Double Axis

Yavuz Ege, Osman Kalender, and Sedat Nazlibilek

***Abstract*—In this paper, a new rotating magnetic stirrer system that is controlled by a programmable-integrated-circuit (PIC) microcontroller and can stir in double axis is developed. In contrast to making a stirring action only at one point, as in the case of traditional electromagnetic stirrers, the system that is developed can rotate at two separate axes. One of the rotations is around the axis of the magnetic stir bar itself, and the other is over a circle defined by a rotating magnetic field. That is, the stirrer makes two rotational motions. This is the main contribution of this paper. The magnetic stirrer system is designed as a three-phase system, and a sinusoidal ramp signal is applied to the phases as the supply voltage. During the design stage, the mathematical model of the system was obtained, and the parameters affecting the design were determined. Based on these parameters, a parameter set was established. This parameter set can be used for subsequent design studies of the system. A PIC-based control circuit is used to control the frequency of the supply voltage. The structure of the double-rotating electromagnetic stirring system is explained. The physical conditions affecting the double-axis rotational motion of the magnetic stir bar are discussed in detail. It was observed that a more homogeneous stirring process could be achieved with this kind of double-axis rotation.**

***Index Terms*—Electromagnetic stirrer, magnetic stir bar, programmable-integrated-circuit (PIC) microcontroller, rotating magnetic field.**

I. Introduction

IN INDUSTRIAL applications for stirring liquid products having various densities, a pair of magnets fixed to the rotor of a traditional electrical motor is used. In these types of magnetic stirrers called motorized stirrers, the bar magnet making the stirring action rotates, depending upon the pair of magnets connected to the motor, and the liquid in which the stir bar is immersed can be stirred [1]–[3]. However, a magnet rotating, particularly at lower speeds inside a liquid, leaves the rotation center and sticks to one of the magnets providing the rotation. This situation negatively affects the stirring process.

In recent years, depending on the application area, either linear or rotational magnetic stirrer can be used for a stirring process [4]–[15]. Rotational stirrers are actually axial flux synchronous motors [7]–[20]. The main difference of the magnetic stirrer from a conventional motorized stirrer is that there is no physical connection between the magnetic stir bar serving as the rotor and the source of the magnetic field. As the magnetic field rotates, the magnetic stir bar inside the liquid also rotates following the rotation of the magnetic field. However, because this rotational motion takes place at the center of the field, the liquid inside the cup is well stirred around the center, but it is not as good as that at the center at the outer region [6]. As a result, the liquid cannot be stirred homogeneously. To be able to obtain a homogeneous mixture, the magnetic stir bar has to be effective at both the central and outer regions. It is planned to design a system that can stir the liquid in both regions and provide a homogeneous mixture. The rotational actions of a magnetic stir bar look like the rotational motions of the Earth. When the bar rotates at its axis, it also makes a motion over a circle around the axis of the cup. The radius of the circle over which the rotation of the bar takes place is chosen according to the cup used. In this paper, we explain the work related to the development of such a novel rotational magnetic stirrer having a programmable-integrated-circuit (PIC)-controlled supply unit forcing the stir bar to make the necessary double-axis rotational motion. The structure of the system and the experimental results are explained in Section II. The mathematical theory related to the double-axis rotational action is given in Section III. The theoretical results are given in Section IV. An overall discussion is made in Section V as conclusion.

II. System Structure and Experimental Results

The double-rotation magnetic stirrer developed in this paper is shown in Fig. 1(a). The electromagnetic stirrer that is designed as a three-phase system creates a rotating magnetic field by means of a sinusoidal supply voltage obtained by the PIC-controlled supply unit. The waveform of this three-phase supply voltage is shown in Fig. 1(b). The frequency of the supply voltage can be adjusted from the control unit.

When the supply voltage is applied to any coil of the stirrer seen in Fig. 1(a), both the four iron cores and the iron ring are magnetized, as shown in Fig. 2. The directions of magnetization can clearly be seen in Fig. 2. Two of the iron cores behave as N poles, and the other two behave as S poles, depending on the input direction of the current. The iron ring at the center is also magnetized by the effect of the current passing through the coils. Because this iron ring is outside the coil, its direction of magnetization is opposite to that of the iron cores. Although the iron ring is a complete circle, because of the lack of magnetization between two regions, it behaves as two U-type magnets, in which their opposite poles are matched against each other.

When a glass jar filled with a liquid is located at the stirrer's stator part and a magnetic stir bar having a length of L is

Manuscript received April 2, 2009; revised August 26, 2009; accepted September 26, 2009. Date of publication October 20, 2009; date of current version June 11, 2010.

Y. Ege is with the Necatibey Education Faculty and the Department of Physics, Balikesir University, Balikesir 10100, Turkey (e-mail: yege@balikesir.edu.tr).

O. Kalender is with the Department of Technical Sciences, Turkish Military Academy, Ankara 06100, Turkey (e-mail: okalender@kho.edu.tr).

S. Nazlibilek is with the Communications and Electronics Systems Branch, Turkish General Staff, Ankara 06100, Turkey (e-mail: snazlibilek@tsk.mil.tr).

Color versions of one or more of the figures in this paper are available online at http://ieeexplore.ieee.org.

Digital Object Identifier 10.1109/TIE.2009.2034676

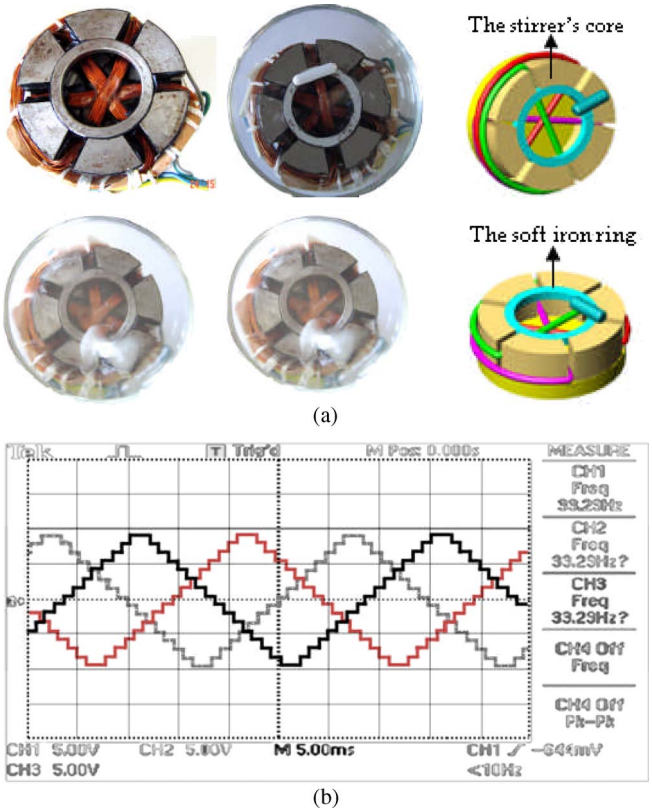

Fig. 1. (a) Structure of the magnetic stirrer. (b) Supply-voltage waveform.

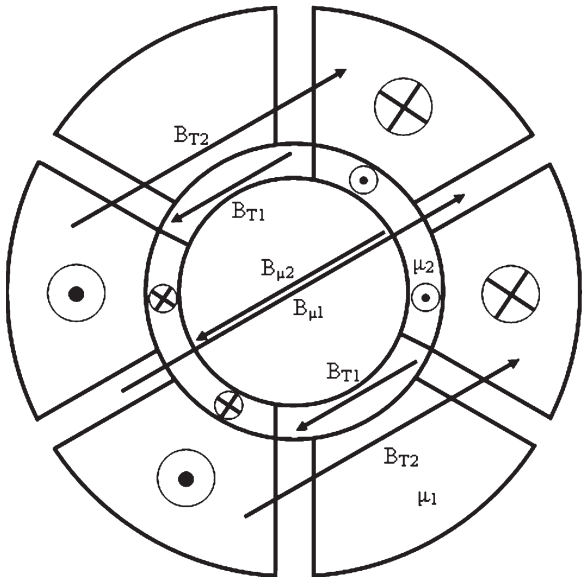

Fig. 2. Directions of magnetization.

immersed in the liquid in the jar, the stir bar is subjected to two magnetic fields $B_{\mu 1}$ and $B_{\mu 2}$. If $|B_{\mu 1} - B_{\mu 2}| \gg 0$, then the stir bar makes a rotational action at the center (around its axis). However, if $B_{\mu 1} - B_{\mu 2} \cong 0$, then the stir bar is pulled to B_{T1} and located at the unmagnetized section of the iron ring, i.e., in other words, on the region where the flux lines complete each other (see Fig. 3). When the supply voltage is applied to the phase coils, the stir bar rotates both at its axis and around

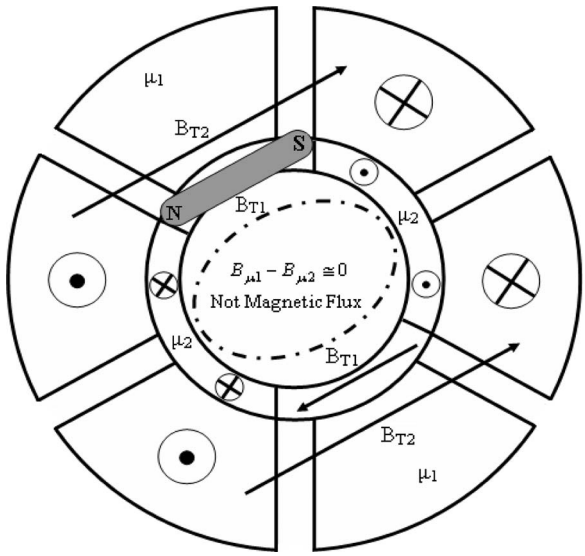

Fig. 3. Initial position of the magnetic stir bar before starting the double-axis rotational motion.

TABLE I
APPROPRIATE FREQUENCIES AND NUMBER OF ROTATIONS FOR THE DOUBLE-AXIS ROTATIONAL MOTION ACCORDING TO THE TYPE OF THE STIR BAR (EXPERIMENTAL MEASUREMENT)

The length of stir bar (cm)	The mass of stir bar (g)	The operation frequency (Hz)	N_1 (The number of rotations of the stir bar around the iron ring)
1.4	2.04	1-6	42
2.2	2.71	1-6	120
2.8	3.91	1-6	196

the magnetized iron ring, similar to the Earth rotating at its axis, as well as the Sun.

As seen from (1), the amplitude of the current passing through the coils is inversely proportional to the frequency of the triangular wave applied to the coils [21]. Therefore, in our experimental study, the frequency of the applied supply voltage is changed in order to change the magnitudes of fields $B_{\mu 1}$ and $B_{\mu 2}$

$$i_{\max} = \frac{V_0}{\sqrt{(2\pi f L)^2 + r_0^2}}. \tag{1}$$

In this equation, V_0 is the voltage applied to the coils, f is the frequency, r_0 is the internal resistance of the coils, and L is the self-induction. Therefore, as the frequency increases, the amplitude of current $i_{\max}$ decreases, and the magnitudes of magnetic fields $B_{\mu 1}$ and $B_{\mu 2}$ that are directly proportional to current $i_{\max}$ decrease. As a result, the $B_{\mu 1} - B_{\mu 2}$ difference approaches to zero. Because of this reason, the magnetic stir bar is released from the total effect of magnetic fields $B_{\mu 1}$ and $B_{\mu 2}$ at a certain frequency and pulled to the direction of B_{T1} where the flux lines complete each other (Fig. 3). However, it is observed that the magnetic stir bar still stays at that region when the value of frequency becomes larger than the value for which the double rotation occurs because of the difficulty to overcome the friction by the stir bar. Three different stir bars in lengths and masses are used. The frequencies determined for the double rotation are listed in Table I.

The values of the frequencies observed in the experiments are only valid for the parameters of the stirrer that are used during the experiments. If it is planned to design a stirrer for a specific type of industrial application, an estimated value on the frequency for which the magnetic stir bar performs a double-axis rotational motion has to be determined during the manufacturing phase, depending on the properties of the materials to be used in production. Notice that the double-axis rotational motion of the stir bar is achieved in low frequencies in this paper, as seen in Table I. The reason for this is that the magnetic permeability of the ring is greater than that of the material used to manufacture the stirrer core. Therefore, in this paper, it is found that the difference between $B_{\mu 1}$ and $B_{\mu 2}$ is about zero (i.e., $B_{\mu 1} - B_{\mu 2} \cong 0$) before the frequency has been changed. It is necessary to select appropriate values for $B_{\mu 1}$ and $B_{\mu 2}$ for achieving double-axis rotational motion. One of the methods that were applied previously is to adjust the frequency of the supply voltage. However, there are some other ways for changing the magnitudes of magnetic fields $B_{\mu 1}$ and $B_{\mu 2}$. One of the aims of this paper is the determination of all the physical factors affecting the double-axis rotational motion of the stir bar, and the other is the understanding of the mechanics of this motion.

III. Mathematical Theory for Double-Axis Rotational Motion

For a magnetic stir bar to be able to do a double-axis rotational motion, as mentioned earlier, the values of $B_{\mu 1}$ and $B_{\mu 2}$ have to be brought to appropriate magnitudes. Therefore, first of all, the relations giving these magnitudes of magnetic fields need to be determined. In this paper, the relation giving the magnitude of the magnetic field created by the current passing through the coils that are wound around each iron core part that is at a height of h from the surface of the core is determined.

The magnetic-field magnitude created at a distance (x_0, y_0) from the current input terminal of a wire with finite length of L can be calculated by [22], [23]

$$B = \frac{\mu_0 i_{\max}}{4\pi \mathrm{x}_0}\left[\frac{y_0}{\sqrt{x_0^2+y_0^2}} - \frac{y_0 - L}{\sqrt{(y_0-L)^2+x_0^2}}\right]. \quad (2)$$

If the diameter is large and the number of phases is increased, then the curvature of the inner and outer surfaces of each core part decreases, and it can be considered as planar. Then, the magnetic field created at point A by the coil that is wound around such a core part is equal to the sum of the magnetic fields created at the same point by four wires that are finite but at different lengths. However, the magnetic stir bar interacts only with the perpendicular component of the magnetic field created at point A by the coil. The other parallel component is around zero.

Therefore, when a single coil is wound around one core part, the relation giving the magnitude of the magnetic field created at point A by the four wire parts has to be obtained separately for each of them. Let us find first of all the perpendicular component of the magnetic field at point A of the finite wire with a length of c.

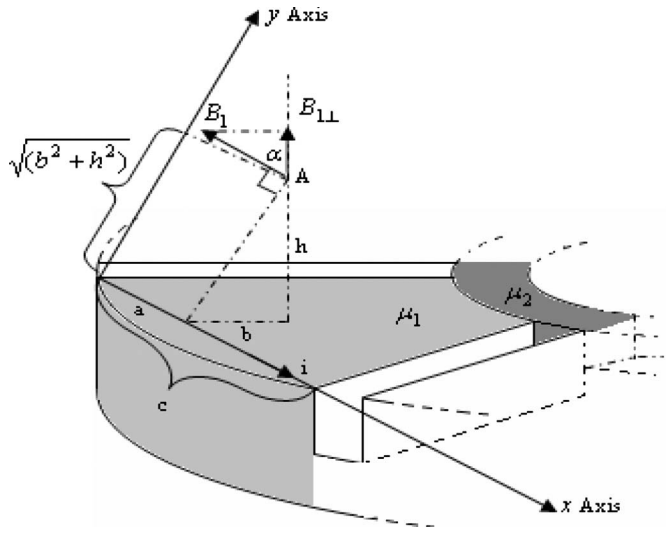

Fig. 4. Magnetic field at point A of the wire with a length of c carrying a current i.

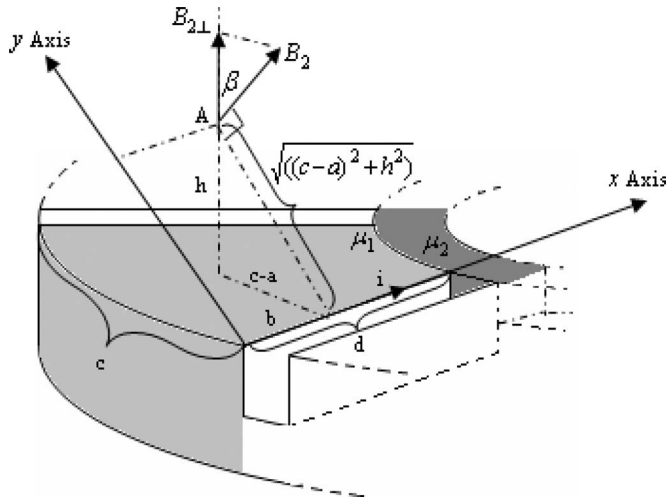

Fig. 5. Magnetic field at point A of the wire with a length of d carrying a current i.

In Fig. 4, a vectorial representation of the magnetic field created by this wire is shown. The distance from the end point where the current enters the wire with a length of c to point A is (a, $\sqrt{b^2+h^2}$). Therefore, using (2), $B_{1\perp}$ can be determined from

$$B_{1\perp} = \frac{\mu_1 i_{\max} \mathrm{b}}{4\pi \mathrm{a}\sqrt{b^2+h^2}} \times \left[\frac{\sqrt{b^2+h^2}}{\sqrt{a^2+b^2+h^2}} - \frac{\sqrt{b^2+h^2}-c}{\sqrt{(\sqrt{b^2+h^2}-c)^2+a^2}}\right]. \quad (3)$$

Now, let us find the perpendicular component of the magnetic field of the finite wire with a length of d. In Fig. 5, the vectorial representation of this magnetic field is shown.

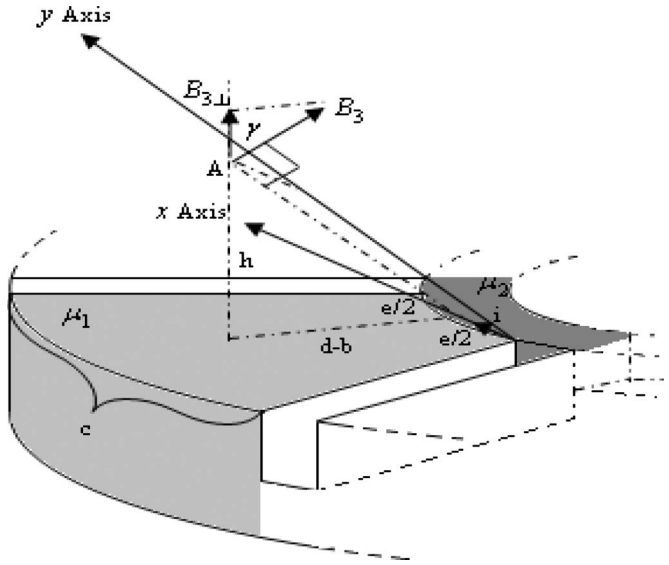

Fig. 6. Magnetic field at point A of the wire with a length of e carrying a current i.

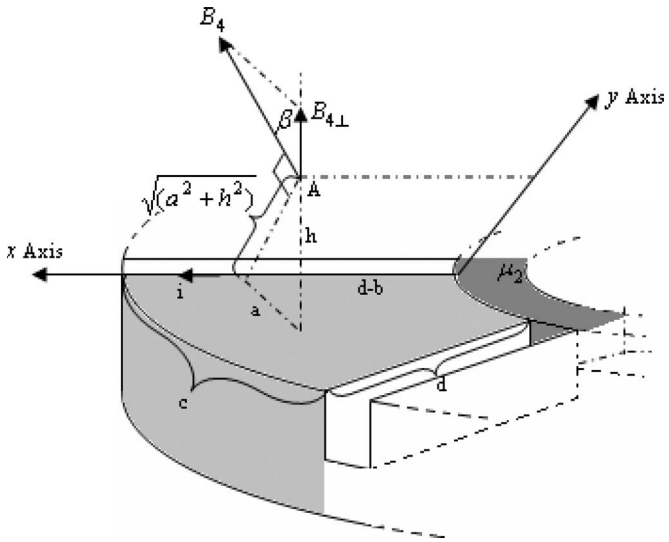

Fig. 7. Magnetic field at point A of the wire with a length of d carrying a current i.

As seen in Fig. 5, the distance from the end point where the current enters the wire to point A is (b, $\sqrt{((c-a)^2+h^2)}$). Therefore, following the same procedure, the perpendicular component $B_{2\perp}$ can be obtained as follows:

$$B_{2\perp} = \frac{\mu_1 i_{\max}(\mathrm{c}-\mathrm{a})}{4\pi \mathrm{b}\sqrt{(c-a)^2+h^2}} \times \left[\frac{\sqrt{(c-a)^2+h^2}}{\sqrt{b^2+(c-a)^2+h^2}} - \frac{\sqrt{(c-a)^2+h^2}-d}{\sqrt{\left(\sqrt{(c-a)^2+h^2}-d\right)^2+b^2}} \right]. \quad (4)$$

Similarly, the magnetic field values created by wires d and e with finite length through which the current passes (Figs. 6 and 7) can be found by taking into account the distances between the point where the currents enter the wire and point A by using

$$B_{3\perp} = \frac{2\mu_1 i_{\max}(\mathrm{d}-\mathrm{b})}{4\pi \mathrm{e}\sqrt{(d-b)^2+h^2}} \times \left[\frac{\sqrt{(d-b)^2+h^2}}{\sqrt{(d-b)^2+\left(\frac{e}{2}\right)^2+h^2}} - \frac{\sqrt{(d-b)^2+h^2}-e}{\sqrt{\left(\sqrt{(d-b)^2+h^2}-e\right)^2+\left(\frac{e}{2}\right)^2}} \right] \quad (5)$$

$$B_{4\perp} = \frac{\mu_1 i_{\max}\mathrm{a}}{4\pi(\mathrm{d}-\mathrm{b})\sqrt{a^2+h^2}} \times \left[\frac{\sqrt{a^2+h^2}}{\sqrt{(d-b)^2+a^2+h^2}} - \frac{\sqrt{a^2+h^2}-d}{\sqrt{(\sqrt{a^2+h^2}-d)^2+(d-b)^2}} \right]. \quad (6)$$

Therefore, if the number of phases is k and the number of turns is N, then it can be written for $B_{\mu 1}$ as

$$B_{\mu 1} = (2k-2)N[B_{1\perp}+B_{2\perp}+B_{3\perp}+B_{4\perp}]. \quad (7)$$

The currents passing through the coils that are wound around the iron core part can also create a magnetic field above the surface of the iron ring at a height of h. Now, let us determine the relation giving the magnitude of this magnetic field.

The perpendicular component $B_{5\perp}$ whose vector diagram is shown in Fig. 8 can be given by

$$B_{5\perp} = \frac{\mu_2 i_{\max}\left(d+\frac{f}{2}\right)}{4\pi \mathrm{a}\sqrt{\left(d+\frac{f}{2}\right)^2+h^2}} \times \left[\frac{\sqrt{\left(d+\frac{f}{2}\right)^2+h^2}}{\sqrt{a^2\left(d+\frac{f}{2}\right)^2+h^2}} - \frac{\sqrt{\left(d+\frac{f}{2}\right)^2+h^2}-c}{\sqrt{\left(\sqrt{\left(d+\frac{f}{2}\right)^2+h^2}-c\right)^2+a^2}} \right]. \quad (8)$$

Similarly, the perpendicular component $B_{6\perp}$ whose vector diagram is shown in Fig. 9 can be found from

$$B_{6\perp} = \frac{\mu_2 i_{\max} f}{4\pi \mathrm{e}\sqrt{\left(\frac{f}{2}\right)^2+h^2}} \times \left[\frac{\sqrt{\left(\frac{f}{2}\right)^2+h^2}}{\sqrt{\left(\frac{f}{2}\right)^2+\left(\frac{e}{2}\right)^2+h^2}} - \frac{\sqrt{\left(\frac{f}{2}\right)^2+h^2}-e}{\sqrt{\left(\sqrt{\left(\frac{f}{2}\right)^2+h^2}-e\right)^2+\left(\frac{e}{2}\right)^2}} \right]. \quad (9)$$

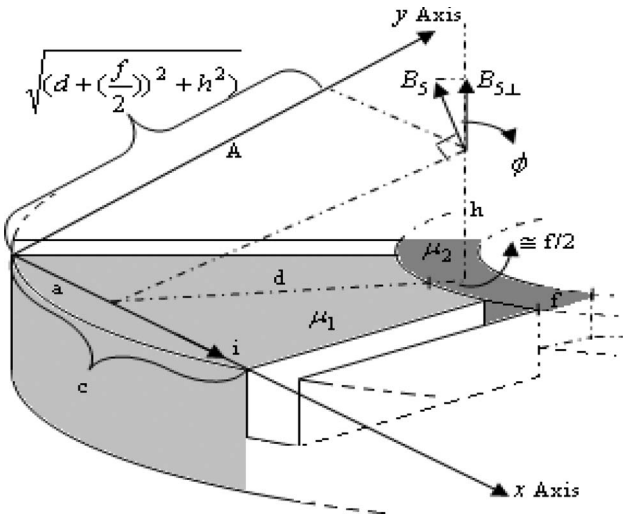

Fig. 8. Magnetic field at the height of h over the wire with a length of c carrying a current i.

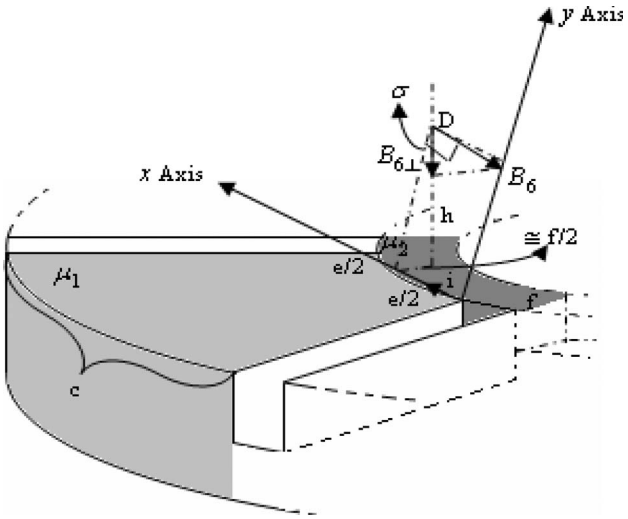

Fig. 9. Magnetic field at the height of h over the wire with a length of e carrying a current i.

The magnetic fields created at point D of the two wires with length d of the coil cancel each other because of the opposite currents passing through the wires. If the number of phases is called k and the number of turns is N, then $B_{\mu 2}$ can be written as

$$B_{\mu 2} = (2k-2)N[B_{6\perp} - B_{5\perp}]. \tag{10}$$

As noted from the relations given earlier, in order to obtain closer values for $B_{\mu 2}$ and $B_{\mu 1}$, it is not sufficient to decrease the value of the current only by increasing frequency f. It may be better to choose the magnetic permeability of the ring (μ_2) to be greater than that of the core. For example, as in this paper, because of the magnetic permeabilities of the materials selected appropriately, the difference between the magnetic fields becomes around zero (i.e., $B_{\mu 1} - B_{\mu 2} \cong 0$), even at an application frequency of 1 Hz. The total magnetic field being around zero means that the magnetic flux lines at the center of the stirrer disappear by losing their linearities. In this case,

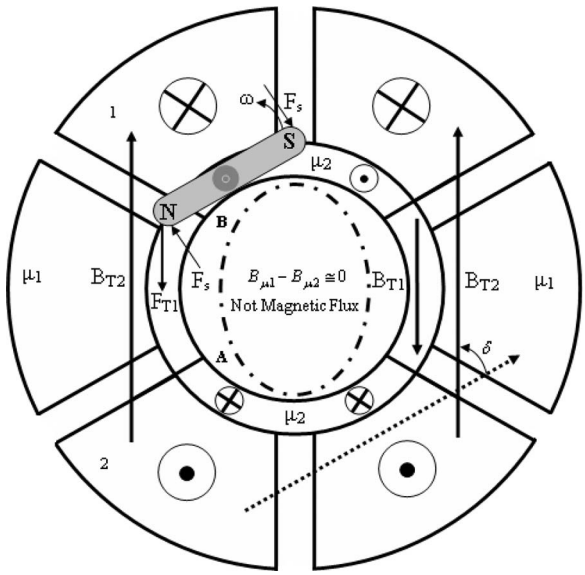

Fig. 10. Forces acting on the magnetic stir bar by the change of direction of magnetic field B_{T1}.

the magnetic stir bar enters the region where the B_{T1} field is effective, and it does not disturb the linearity of the magnetic field lines that trace a closed path. Here, the magnitudes of magnetic fields B_{T1} and B_{T2} can be calculated from the following:

$$\begin{aligned} B_{T2} &= 2N[B_{1\perp} + B_{2\perp} + B_{3\perp} + B_{4\perp}] \\ B_{T1} &= 2N[B_{6\perp} - B_{5\perp}]. \end{aligned} \tag{11}$$

The magnetic stir bar is subjected to two different forces as a result of change in the direction of field vector B_{T1} by an amount of angle δ with the change of phase. Force F_{T1} gives the stir bar both a translational and a rotational movement. Force F_S is the friction force of the liquid inside the cup acting on the stir bar in the opposite direction to the rotation. The magnitudes of these forces can be obtained from [24]

$$\begin{aligned} F_{T1} &= \frac{Br_{1x}^2 B_{T1} \sin\delta}{2} \\ F_s &= \eta\left(mg + \left(\frac{\rho V_s g}{A_k} \times A\right) - \rho g V_c\right) \end{aligned} \tag{12}$$

where B is the magnetic flux density at the poles of the rod magnet, r_{1x} is the distance between the N pole of the stir bar and the field center of the number-2 core part, ρ is the density of the liquid to be stirred, η is the friction coefficient between the magnetic stir bar and the surface of the cup, V_s is the volume of the liquid, A_k is the surface area of the bottom of the cup, A is the area of the upper surface of the stir bar, and V_c is the volume of the magnetic stir bar.

As seen from Fig. 10, on the one hand, it is required that the condition in (13) must hold in order that the stir bar rotates at its axis with an angular velocity

$$F_{T1}\sin\delta - F_S > 0. \tag{13}$$

On the other hand, if it is assumed that the magnetic effects of two N poles near the S pole of the stir bar cancel each other,

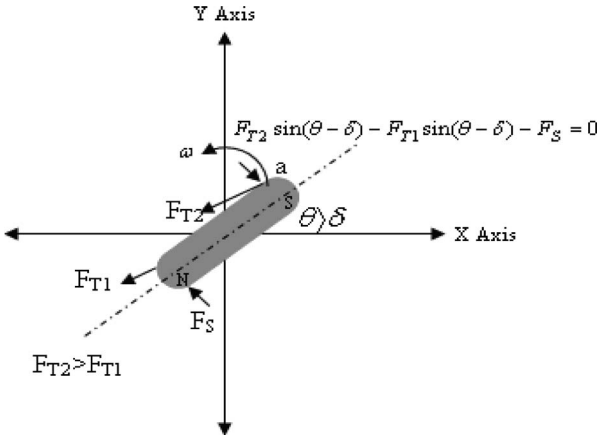

Fig. 11. Forces acting on the stir bar when it is in position a.

then the magnetic stir bar is translated to the iron ring of radius r by force $F_{T1}\cos\delta$. When the magnetic stir bar rotates at an angle of δ, force $F_{T1}\sin\delta$ disappears. However, the magnetic stir bar may rotate by angle θ until the friction force damps the energy gained. After the stir bar has rotated by angle δ, the forces shown in Fig. 11 become effective. In this experimental work, angular velocity ω reached after the rotation by angle δ remains constant. From Newton's law of inertia, the following equation must be satisfied in order that the angular velocity ω of the magnetic stir bar does not decrease:

$$F_{T2}\sin(\theta-\delta)-F_{T1}\sin(\theta-\delta)-F_S=0 \qquad (14)$$

in which force F_{T2} can be obtained from

$$F_{T2}=\frac{Br_{2x}^2 B_{T2}\sin\delta}{2}. \qquad (15)$$

The r_{2x} in (15) is the distance between any one of the poles of the stir bar and the center of field B_{T2}.

The positions of the motions of the magnetic stir bar after this movement are shown in Fig. 12.

The magnetic stir bar makes a complete tour by taking positions a, b, c, d, and e in sequence, and at the same time, it takes the direction of field B_{T1} by a translational motion over the iron ring. However, when the stir bar is at position c, the following condition must be met in order that angular velocity ω does not decrease (Fig. 13):

$$F_{T1}\sin(\theta-\delta)-F_{T2}\sin(\theta-\delta)-F_S=0. \qquad (16)$$

If no phase change occurs after the magnetic stir bar has taken the position e shown in Fig. 12, in other words, if field B_{T1} does not change its direction, then it remains in the last direction of field B_{T1}. If the field changes its direction when the stir bar comes exactly at position e, the motion of the magnetic stir bar with angular velocity ω will continue. Therefore, the settling time of the stir bar to the last position after one or several complete tours has to be the same with the time of the phase change. For this reason, the magnetic stir bar can do double rotation in certain frequencies.

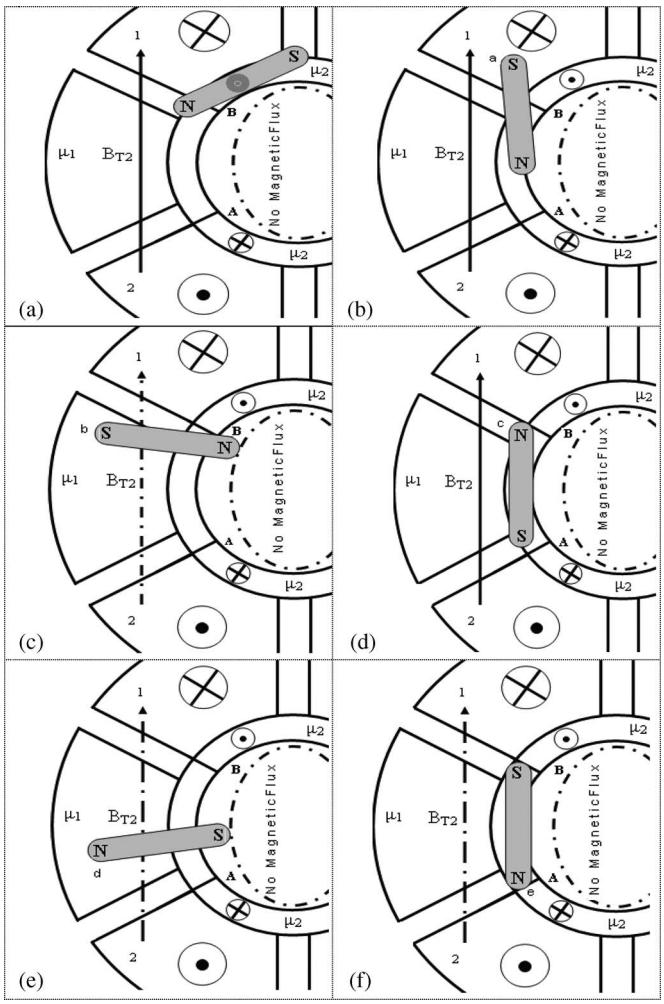

Fig. 12. Complete tour of the magnetic stir bar. (a) Position a. (b) Position b. (c) Position c. (d) Position d. (e) Position e. (f) Position f.

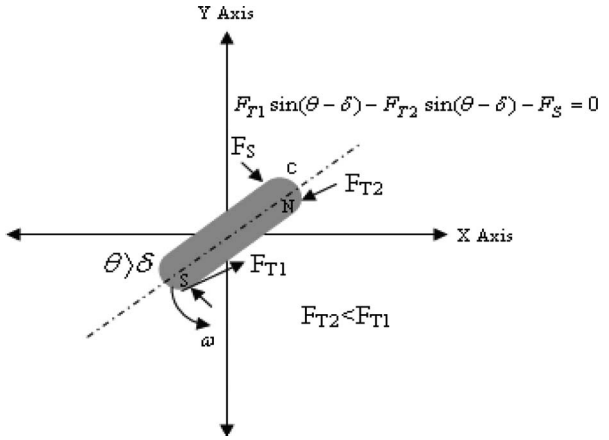

Fig. 13. Forces acting on the magnetic stir bar when it is in position c.

IV. Theoretical Results

The characteristic values related to the stirrer and the magnetic stir bars that are developed in this paper can be seen in Table II. The forces applied to the magnetic stir bars during the double-axis rotational motion, the linear velocity, and the number of rotations when the applied frequency is 6 Hz are given in Table III.

TABLE II
ALL VARIABLES AND VALUES

Variable	Name of the Variable	Value of the Variable					
μ_1	Permeability of the stirrer's core	0.565×10^{-4} Tm/A					
μ_2	Permeability of the soft iron ring	4.028×10^{-4} Tm/A					
i_{max}	The coil current	1.721 A					
f	Application frequency	1-7 Hz					
L	Self-induction coefficient of the coil	0.0056 H					
V_0	Voltage of the coil	1.74 V					
r_0	Internal resistance of the coil	1.56 Ω					
k	Number of Phases	3					
a	Core parameter of the stirrer	0.015 m					
b	Core parameter of the stirrer	0.0155 m					
c	Core parameter of the stirrer	0.03 m					
d	Core parameter of the stirrer	0.0305 m					
e	Core parameter of the stirrer	0.0145 m					
f	Core parameter of the stirrer	0.005 m					
h	Thickness of the jar	0.004 m					
N	Number of turns	88					
ρ	The liquid density	1000 kg/m^3					
η	The friction coefficient	0.00003					
V_s	Volume of the liquid	0.0005 m^3					
l	The lengths of the stir bar	Type 1	0.028 m	Type 2	0.022 m	Type 3	0.014 m
B	Magnetic flux density of the stir bar	Type 1	0.01231 T	Type 2	0.003702 T	Type 3	0.001502 T
m	The mass of the	Type 1	0.00391 kg	Type 2	0.00271 kg	Type 3	0.00204 kg
A	The top view surface area of the stir bar	Type 1	2.015×10^{-4} m^2	Type 2	1.583×10^{-4} m^2	Type 3	1.007×10^{-4} m^2
V_c	The volume of the magnetic stir bar	Type 1	1.413×10^{-6} m^3	Type 2	1.107×10^{-6} m^3	Type 3	0.702×10^{-6} m^3
r_{1x}	The distance of the N pole of the stir bar to the No.2 core pole	Type 1	0.029 m	Type 2	0.037 m	Type 3	0.045 m
A_k	Bottom area of the jar	7.85×10^{-3} m^2					
r_{2x}	The distance of the S pole of the stir bar to the No.2 core pole	Type 1	0.011 m	Type 2	0.017 m	Type 3	0.025 m

TABLE III
APPLIED FORCES ON THE STIR BARS DURING THE DOUBLE-AXIS ROTATIONAL MOTION, LINEAR VELOCITY, AND NUMBER OF ROTATIONS FOR 6 HZ (THE RESULTS OBTAINED FROM THE CALCULATIONS FOR THE MATHEMATICAL MODEL)

The type of the stir bar	B μ_1 -B μ_2 (T) The condition for double-axis rotation	F_1 (N) Resultant force (rotational)	F_2 (N) Resultant force (translational)	ϑ (m/s) Linear velocity	N_1 Number of tours over the iron ring of the stir bar
Type 1	$0.00006 \cong 0$	8.162×10^{-8}	11.297×10^{-7}	0.00812	40
Type 2	$0.00006 \cong 0$	1.582×10^{-8}	6.315×10^{-7}	0.00381	125
Type 3	$0.00006 \cong 0$	0.308×10^{-8}	3.786×10^{-7}	0.00154	200

TABLE IV
BOUNDARY VALUES OF THE VARIABLES/PARAMETERS AFFECTING THE SYNCHRONIZATION CONDITIONS FOR DOUBLE-AXIS MOTION AND THE COMPLIANCE OF MATHEMATICAL AND EXPERIMENTAL RESULTS

Variable / parameters	Maximum values of variables in the mathematical model	Maximum values of variables in the experimental measurements	Frequencies	Double-axis motion	Without motion
ρ	1191 kg/m^3	1200 kg/m^3	6 Hz	Under 1200 kg/m^3	Above 1200 kg/m^3
h	0.00445 m	0.0048 m	6 Hz	Under 0.0048 m	Above 0.0048 m
N	77	78	6 Hz	Above 78	Under 78
V_s	0.00059 m^3	0.0006 m^3	6 Hz	Under 0.0006 m^3	Above 0.0006 m^3
A_k	0.00672 m^2	0.0068 m^2	6 Hz	Above 0.0068 m^2	Under 0.0068 m^2

As seen from Table III, there is no magnetic field at the central region of the stirrer. For this reason, a double-axis rotational motion caused by the translational and rotational forces acting on the magnetic stir bar can be observed. It is obvious that the stir bar can reach a linear velocity by the effect of these forces. It easily can be noticed that the experimental results comply with the calculations related to the linear velocities and number of rotations of the stir bar at its axis during rotation around the ring at one complete tour.

As shown in Table I, when the applied frequency is increased above 6 Hz, the resultant force causing the rotation of the stir bar seen in Table III becomes negative (13). That is, the friction force becomes dominant, and hence, the double-axis rotation stops. This phenomenon is observed in this paper.

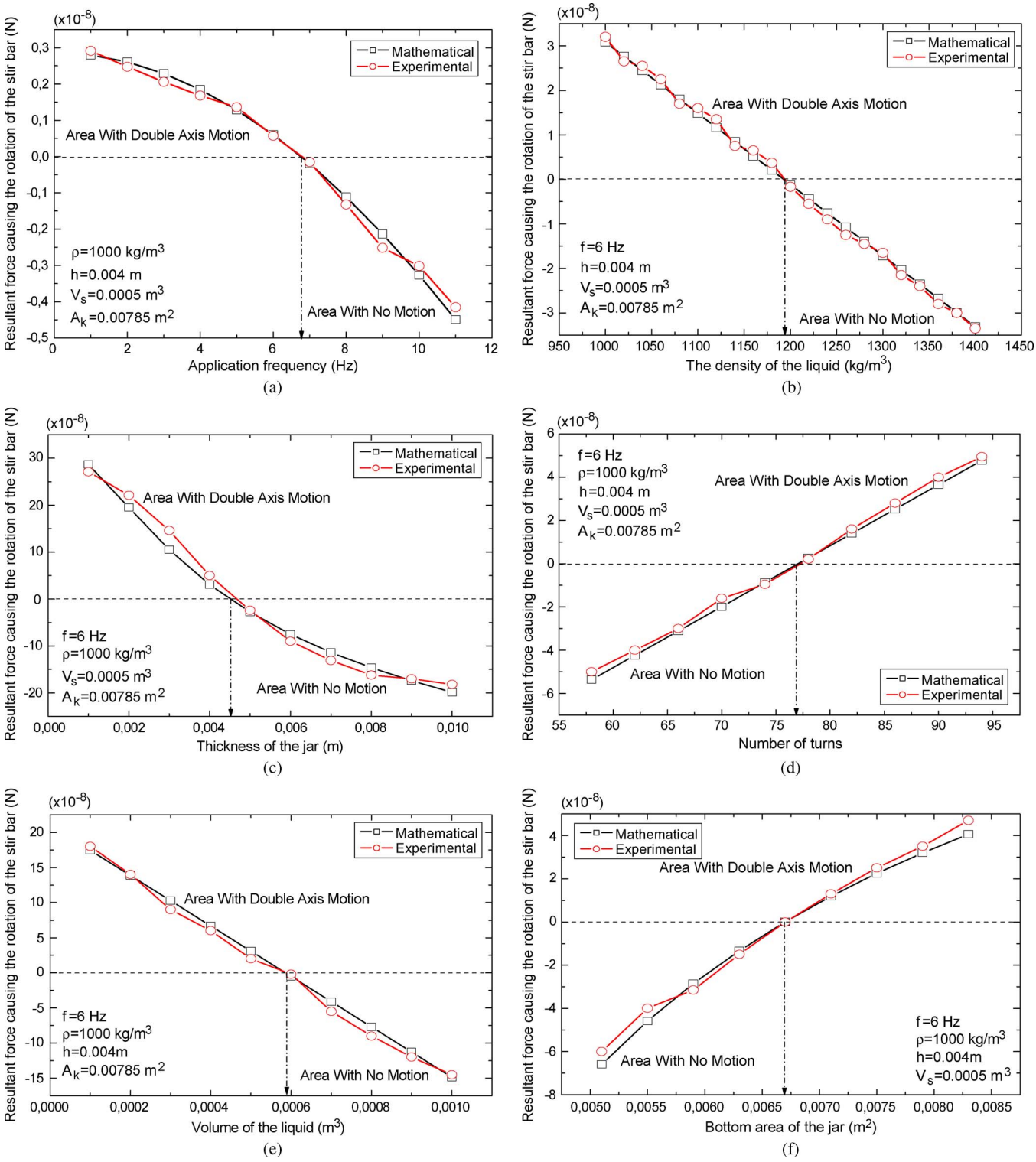

Fig. 14. Change of the resultant force causing the rotation of the type-3 magnetic stir bar with respect to (a) frequency, (b) density of the liquid, (c) height, (d) number of turns, (e) volume of the liquid, and (f) cross section of the glass jar.

Furthermore, when the number of tours over the iron ring of the stir bar (N_1) obtained from the experiments (Table I) and the results calculated from the mathematical model (Table III) are compared, it can be claimed that the model is reasonably realistic.

It can be seen from Table II that the double-axis rotational motion of a magnetic stir bar within a rotating magnetic field over a soft-iron ring may be dependent on 27 different variables and parameters. Eight of them (i.e., μ_1, μ_2, a, b, c, d, e, and f) belong to the core of the stirrer.

In addition to these variables and parameters, an appropriate value of the application frequency determining $i_{\max}$, when adjusted so that the total value of magnetic fields $B_{\mu 1}$ and $B_{\mu 2}$ is equal to zero, will improve the possibility of occurrence of

double-axis motion. For the stirrer that is realized and used in this paper, the magnetic field intensity values $B_{\mu 1}$ and $B_{\mu 2}$ calculated from the mathematical model and obtained from the experiments are equal to each other. One other important result obtained from this paper is that the frequency of the supply voltage not only decreases the magnitudes of B_{T1} and B_{T2} but also causes the phase-change time to be shortened. If there is a lack of synchronization between the phase-change time and the time needed for the stir bar to turn one or several times and translated over the iron core and taking the direction of field B_{T1}, then it will not be possible that the stir bar can achieve a double-axis rotational motion. For synchronization

$$(2N_1k)\frac{1}{f} = \frac{\pi\ell}{\vartheta},$$

$$\vartheta = \sqrt{2 \times \frac{F_{T1}\sin\delta - F_s}{m} \times \left(\frac{3.14}{3} \times \frac{\lambda}{2}\right)} \quad (17)$$

where the first part of these equations is for the complete tour over the iron ring. ℓ is the length of the magnetic stir bar, ϑ is the linear velocity of the magnetic stir bar, k is the number of phases, and N is the number of complete tours over the iron ring by the magnetic stir bar.

Variables such as liquid density, thickness of the jar, number of turns of the stirrer coil, volume of the liquid, and area of the bottom of the jar are all effective for the synchronization condition of a double-axis motion given in (17). In the experimental work, the effects of these variables were evaluated for three types of stir bars, and the results obtained are given in Table IV. These five of 27 variables given in Table II were changed in a predetermined order, and the synchronization times of the five variables/parameters and their capability for double-axis rotational motion were attempted to be determined.

In addition, the boundary values that these variables/parameters could get were determined by the use of the mathematical model that is developed and the experimental measurements that are carried out. As seen in Fig. 14, both of the results are compliant with each other.

V. Conclusion

In this paper, the design of a magnetic stirrer performing double-axis rotational motion has been achieved. The design parameters and an appropriate parameter set for a working prototype have been determined. The set of parameters affecting the design of the stirrer is as follows: the distance d that effects the magnitude of B_{T1}, the distance f that effects the magnitude of B_{T2}, the number of phases, the magnetic permeability of the cores, the number of turns, the self-induction coefficient and the internal resistance of the coil, the length of the magnetic stir bar, the top-view surface area of the stir bar, the distances r_{1x} and r_{2x}, the magnetic flux density of the stir bar, the frequency of the supply voltage, the distance of the magnetic stir bar to the stirrer (h), the height of the liquid, and the density of the liquid.

During the design and implementation phase of similar systems, first of all, the linear velocity must be obtained from (17), and then, using (13) and (14), F_{T1} and F_s shall be calculated. Also, by using (13) and (16), the magnitudes of B_{T1} and B_{T2} must be determined. Last of all, by using (3)–(12), the type of stirrer and the number of turns that can satisfy these magnetic-field magnitudes must be decided.

References

[1] T. J. Bruno and M. C. Rybowiak, "Vapor entraining magnetic mixer for reaction and equilibrium applications," *Fluid Phase Equilib.*, vol. 178, no. 1/2, pp. 271–276, Mar. 1, 2001.

[2] F. Barbeu, L. Gbahoue, and S. Martemianov, "Energy cascade in a tornado wise flow generated by magnetic stirrer," *Energy Convers. Manage.*, vol. 43, no. 3, pp. 399–408, Feb. 2002.

[3] K. H. Spitzer, G. Reiter, and K. Schwerdtfeger, "Multi-frequency electromagnetic stirring of liquid metals," *ISIJ Int.*, vol. 36, no. 5, pp. 487–492, 1996.

[4] A. Borowski, J. Sartoris, and R. Jurgens, "Use of electromagnetic rotating-field stirrers in a continuous caster," *Stahl Eisen*, vol. 118, no. 1, p. 59, Jan. 1998.

[5] S. Milind and V. Ramanarayanan, "Design and analysis of a linear type electromagnetic stirrer," in *Conf. Rec. 39th IEEE IAS Annu. Meeting*, Oct. 3–7, 2004, vol. 1, pp. 188–194.

[6] O. Kalender and Y. Ege, "A PIC microcontroller based electromagnetic stirrer," *IEEE Trans. Magn.*, vol. 43, no. 9, pp. 3579–3585, Sep. 2007.

[7] F. Marignetti, V. Delli Colli, and Y. Coia, "Design of axial flux PM synchronous machines through 3-D coupled electromagnetic thermal and fluid-dynamical finite-element analysis," *IEEE Trans. Ind. Electron.*, vol. 55, no. 10, pp. 3591–3601, Oct. 2008.

[8] F. Locment, E. Semail, and X. Kestelyn, "Vectorial approach-based control of a seven-phase axial flux machine designed for fault operation," *IEEE Trans. Ind. Electron.*, vol. 55, no. 10, pp. 3682–3691, Oct. 2008.

[9] F. Profumo, Z. Zhang, and A. Tenconi, "Axial flux machines drives: A new viable solution for electric cars," *IEEE Trans. Ind. Electron.*, vol. 44, no. 1, pp. 39–45, Feb. 1997.

[10] M. Aydin, S. Huang, and T. A. Lipo, "Torque quality and comparison of internal and external rotor axial flux surface-magnet disc machines," *IEEE Trans. Ind. Electron.*, vol. 53, no. 3, pp. 822–830, Jun. 2006.

[11] S. Zhang and F. L. Luo, "Direct control of radial displacement for bearingless permanent-magnet-type synchronous motors," *IEEE Trans. Ind. Electron.*, vol. 56, no. 2, pp. 542–552, Feb. 2009.

[12] C.-C. Sung and Y.-S. Huang, "Based on direct thrust control for linear synchronous motor systems," *IEEE Trans. Ind. Electron.*, vol. 56, no. 5, pp. 1629–1639, May 2009.

[13] J. Hur, "Characteristic analysis of interior permanent-magnet synchronous motor in electrohydraulic power steering systems," *IEEE Trans. Ind. Electron.*, vol. 55, no. 6, pp. 2316–2323, Jun. 2008.

[14] M. J. Kamper, R.-J. Wang, and F. G. Rossouw, "Analysis and performance of axial flux permanent-magnet machine with air-cored nonoverlapping concentrated stator windings," *IEEE Trans. Ind. Appl.*, vol. 44, no. 5, pp. 1495–1504, Sep./Oct. 2008.

[15] A. B. Letelier, D. A. Gonzalez, J. A. Tapia, R. Wallace, and M. A. Valenzuela, "Cogging torque reduction in an axial flux PM machine via stator slot displacement and skewing," *IEEE Trans. Ind. Appl.*, vol. 43, no. 3, pp. 685–693, May/Jun. 2007.

[16] A. Parviainen, M. Niemela, and J. Pyrhonen, "Modeling of axial flux permanent-magnet machines," *IEEE Trans. Ind. Appl.*, vol. 40, no. 5, pp. 1333–1340, Sep./Oct. 2004.

[17] S. Javadi and M. Mirsalim, "A coreless axial-flux permanent-magnet generator for automotive applications," *IEEE Trans. Magn.*, vol. 44, no. 12, pp. 4591–4598, Dec. 2008.

[18] W. Y. Lin, L. P. Kuan, W. Yun, and D. Han, "Near optimal design and 3-D finite element analysis of multiple sets of radial magnetic couplings," *IEEE Trans. Magn.*, vol. 44, no. 12, pp. 4747–4753, Dec. 2008.

[19] J. Cao, S. Wang, Y. Zhu, and W. Yin, "Modeling the static vertical force of the core type permanent magnet planar motor," *IEEE Trans. Magn.*, vol. 44, no. 12, pp. 4653–4658, Dec. 2008.

[20] N. Chayopitak and D. G. Taylor, "Performance assessment of air core linear permanent magnet synchronous motors," *IEEE Trans. Magn.*, vol. 44, no. 10, pp. 2310–2316, Oct. 2008.

[21] D. Halliday and R. Resnick, *Fundamental of Physics I*. Ankara, Turkey: Arkadas Yayinevi, 2003, p. 914.

[22] D. Halliday and R. Resnick, *Fundamental of Physics II*. Ankara, Turkey: Arkadas Yayinevi, 1990, p. 141.

[23] O. Gurdal, *Elektromanyetik Alan Teorisi*. Ankara, Turkey: Nobel Yayinevi, 2000, p. 213.

[24] E. Gunduz, *Introduction to Modern Physics*. Izmir, Turkey: Ege Universitesi Fen Fakultesi Yayinlari, 1993, p. 13.

Yavuz Ege was born in Soke, Aydin, Turkey, in 1973. He received the M.S. and Ph.D. degrees from the Department of Physics, Institute of Science, Balikesir University, Balikesir, Turkey, in 1998 and 2005, respectively.

He is currently with the Necatibey Education Faculty and the Department of Physics, Faculty of Arts and Sciences, Balikesir University, where he has been an Assistant Professor since 2008. His research interests are solid physics, magnetism, and power electronics.

Osman Kalender was born in Buyukbahceli Cankiri, Turkey, in 1964. He received the B.S. and M.S. degrees from the Department of Computer and Electronics Education, Faculty of Technical Education, Gazi University, Ankara, Turkey, in 1986 and 1991, respectively, and the Ph.D. degree from the Department of Electrical Education, Faculty of Technical Education, Gazi University, in 2005.

He is currently the Chief of Electric and Electronics Main Discipline, Department of Technical Sciences, Turkish Military Academy, Ankara. His main research interests include generalized electrical machinery, power electronics, and magnetism.

Sedat Nazlibilek received the B.S. and M.S. degrees in electrical engineering from Bosphorous University, Istanbul, Turkey, in 1982 and 1984, respectively, and the Ph.D. degree in electrical engineering from Middle East Technical University (ODTÜ), Ankara, Turkey, in 1993.

He is currently the Chief of the Communications and Electronics Systems Branch, Turkish General Staff, Ankara. He is also a part-time Instructor with the Department of Mechatronics Engineering, Atýlým University, Ankara, and the Department of Technical Sciences, Turkish Military Academy, Ankara. His main interest areas are communications, navigation, and identification. His research areas are control systems theory, intelligent control, mobile sensor networks, and robotics.